Cecilia Occhiuzzi, Nicola D'Uva, Simone Nappi, Amendola Sara, Chiara Gialluca, Valentina Chiabrando, Luigi Garavaglia, Giovanna Giacalone, and Gaetano Marrocco

Radio-Frequency-Identification-Based Intelligent Packaging

Electromagnetic classification of tropical fruit ripening.

Intelligent packaging for food continuously generates informative digital/analog content about the contained products during their entire life span, thus becoming one of the enabling elements of the modern data-driven economy. Packaging shells for fruits, augmented with low-cost wireless sensors for the automatic estimation of the ripening grade, can reduce waste, optimize shelf exposure, suggest when produce should be consumed, and engage customers through enhanced user experiences. Radio-frequency identification (RFID) with sensorless, low-cost labels, empowered with electromagnetic-based intelligence and automatic classification tools, may stimulate the widespread diffusion of this technology. Focusing on avocados, this article presents an experimental characterization of RFID's complex permittivity along with ripening and a near-field numerical model of a passive RFID interrogation system with tagged fruit, aimed at extracting the variation of electromagnetic metrics of the RFID link during ripening. The results are used to design and fabricate an RFID totem for avocado monitoring that, coupled with a properly trained binary tree classifier, is capable of recognizing up to three ripening levels of packaged fruits, with an overall accuracy higher than 85% even if the task is executed by unskilled operators.

Digital Object Identifier 10.1109/MAP.2020.3003212
Date of current version: 5 August 2020

INTRODUCTION

Smart packaging senses, monitors, and communicates the conditions of packed goods to generate information about product quality, safety, and history during production, transport, and storage. Packaging for food, in particular, plays a pivotal role [1] in defining strategies and technological innovations for a new kind of interaction with meat and produce in the widely spreading philosophy of the Internet of Things and, more generally, the data-driven economy. Indeed, in addition to its primary function of preserving food quality, intelligent packaging can provide information about the status of a product, from fields and farms to the final distributor. For this purpose, various chemical–physical indicators, data carriers, and sensors have already been explored [2]. Most of them are related to product freshness and the integrity of the packaging and are intended for temperature-, leakage-, and chemical (acidity, humidity, gas sensor, biosensor)-based applications. Even more innovative solutions are aimed at enhancing the packaging–user interaction [3] to accommodate customers' preferences and lifestyles by enabling anticounterfeiting measures [4], optimizing food's effective shelf life [5], identifying the most convenient time to eat food [6], and suggest cooking and preparation recipes. Suitable markets for this paradigm are those of fish, meat [7], cheese, vegetables, and fruits [6], especially the tropical ones [8], whose business impact is constantly growing. Data carriers traditionally include barcodes in

the packaging and, occasionally, colorimetric indicators [9]. More recently, RFID has begun to represent an added-value technology for producers, distributors, and final customers [10].

RFID technology, especially the communication standard operating in the ultrahigh-frequency (UHF) band (870–970 MHz), has been conceived and developed as the natural evolution of the barcode [11], with applications to modern logistics and the secure management of goods [12]. Compared to a barcode, an RFID tag does not require a line of sight, thus enabling fast, on-the-fly readings. Furthermore, it overcomes the barcode limitation of providing only static, poor information. The possibility of adding sensing capabilities [13], such as temperature [14], gas [15], [16], and humidity [17], to the basic ID function opens interesting scenarios for adopting RFID technology in intelligent packaging for food. Some examples of sensing-based food applications are time–temperature indicators [18], the monitoring of cheese maturation [19], spoilage gas detection [20], and beef quality evaluation [21].

In this article, we exploit the integration of batteryless RFID tags into low-cost intelligent packaging for evaluating the stage of fruit ripening. Without a loss of generality, the proposed electromagnetic platform will be applied to the avocado, which is a climacteric fruit characterized by a particular logistic complexity in defining and managing its optimal ripening conditions. The proposed methodology is, however, general purpose, and its application to other food products is straightforward.

The key point of RFID-based intelligent packaging for ripening monitoring is that the complexity and, accordingly, the cost of the sensing tag to be applied on each piece of fruit should be as low as possible to enable massive adoption. Hence, the RFID tags considered in this article do not integrate any external physical or chemical sensors. The sensor is instead replaced by an electromagnetic intelligence that is moved to the reader side so that the analog electromagnetic response of a tag is exploited as the core of a classification problem. Namely, following the sensorless approach in [13], the tag acts as an electromagnetic transducer: signals received and backscattered by the tag during communication with the reader are affected by changes when the fruit ripens, and thus they provide indirect information about the status of the fruit itself. Electromagnetic signals are then used to feed a classification algorithm based on binary tree analysis to predict the fruit ripening as a level of a discretized scale. The method is nondestructive. Tagged fruits can be interrogated all along the supply chain, individually by using short-range readers and in batches when long-range architectures are exploited. Information about the retrieved ripening stages, along with other relevant features, can be automatically stored in the tag's internal memory. A dynamic label with constantly updated data about the fruit's status and shelf life is then achieved.

RATIONALE

PHYSICAL–CHEMICAL CHANGES DURING RIPENING

Avocado ripening generates mechanical, colorimetric, and chemical variations of the fruit [22]. The main physical modification is fruit softening due to the decrease in cell-to-cell adhesion as a consequence of the action carried out by different enzymes (cellulase, pectin methyl esterase, polygalacturonase, and so forth) that work synergistically [23]. Physical changes contribute to fruit texture; in particular, both the viscosity and the elasticity in fruit tissues change as a function of ripening, with the fruit becoming creamier and less watery in texture. As avocados soften with time, dry matter (DM) is the commonly adopted maturity index [24], but it requires a destructive test. (DM consists of all the constituents of plant and animal material, excluding water.) The visual appearance, which is the only parameter that consumers can evaluate (if we exclude manual squeezing, which should be avoided since it damages the fruit by leaving brown and bruised flesh hidden under the skin), changes as well. For instance, the skin color of the cultivated Hass avocado turns from green to purple/black during ripening.

However, the skin color cannot be considered a reliable single indicator of fruit ripeness, as late-season skin darkening can occur before harvest, so some fruits appear to be ripe even though they are not soft. On the contrary, low-temperature storage to prevent ripening and rot could produce fruits with reduced skin darkening [25]. Accordingly, the skin color can definitely confuse consumers. Finally, avocado ripening also produces physiological modifications of chemical properties, in particular, an increase in the oil concentration and a decrease of the sugar content during storage, which is related to postharvest dehydration [26]. Such chemical and physical variations macroscopically affect the RF dielectric properties [27] of the fruit. The dielectric permittivity and conductivity $\{\epsilon_r, \sigma[S/m]\}$ will therefore vary along with the food spoilage, according to a law that will be experimentally evaluated in the next section, thus providing the physical rationale for an electromagnetic-based monitoring approach.

THE ELECTROMAGNETIC SENSING PROBLEM

If an antenna is placed in close proximity to the fruit (e.g., directly attached to the peel), any variation of the fruit properties will, in turn, produce modifications of the antenna's impedance and radiation gain. By properly exploiting and mastering this phenomenon, a self-sensing, completely sensorless, nondestructive, passive device is therefore obtained, wherein the sensor is the antenna, and the antenna is the sensor. The implementation of this approach in realistic environments and processes has been made possible by RFID [13], which has a joint analog (transmitted and backscattered signals in amplitude and phase) and digital (unique ID code) nature.

An RFID system consists of two components: 1) the tag that will be attached to the fruit, including an antenna and a microchip transponder [an integrated circuit (IC)], and 2) the local querying system (or reader), which remotely energizes the tag and collects data that are reflected back through a backscattering modulation. This article is focused on passive batteryless systems working in the UHF band (860–960 MHz), which have an almost unlimited life, very low cost, and activation ranges of up to 10 m.

Let us denote with $\Re(t)$ the ripening status of the fruit to be monitored by the RFID platform. The following

electromagnetic indicators are returned by the reader that interrogates the tagged avocado:

- the transmitted power $P_{R\rightarrow T}[\Re]$ [decibels with reference to 1 mW (dBm)], the power delivered by the reader to the tag's chip
- the turn-on power $P_{to}[\Re]$ (dBm), the minimum power entering the reader antenna to power up the tag
- the received signal strength indicator (RSSI) [$\Re$] (dBm) related to the backscattered power $P_{R\leftarrow T}$ from the tag to the reader.

Moreover, if new-generation self-tuning ICs (RFID ICs that are capable of automatically adjusting their internal impedance to maximize the power transfer from the tag's antenna) are used [28], the power parameters can be measured with the self-tuning capability enabled or disabled, thus providing additional indicators. Furthermore, even the sensor code itself, which is the digital indicator of the optimal self-tuning state automatically adjusted by the IC, could be considered an additional sensing indicator. Starting from these, several metrics can be then derived, thus giving the electromagnetic fingerprint of the fruit. The problem is, then, estimating the ripening process $\Re(t)$ from that avocado RFID fingerprint by means of automatic classification.

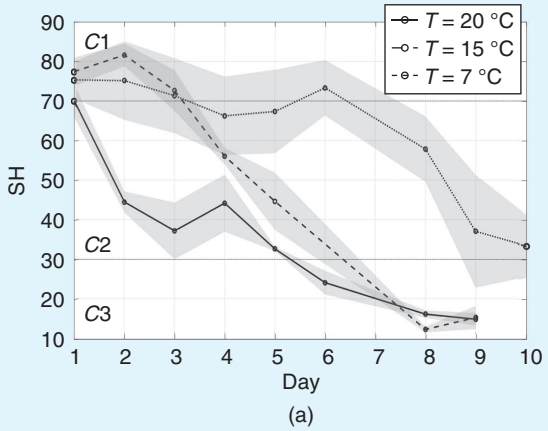

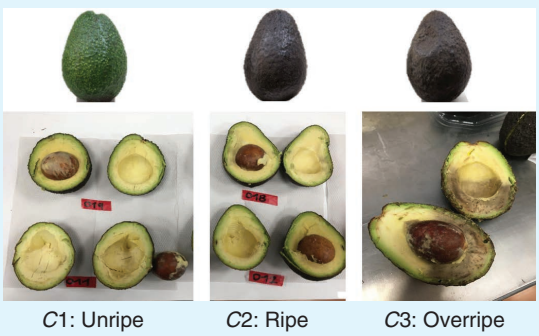

FIGURE 1. (a) The SH versus ripening days for fruits stored at three different environmental conditions {7, 15, 20}°C. The gray area corresponds to the standard deviation. (b) Avocado samples at three relevant ripening stages that are identified in Table 1.

EXPERIMENTAL CHARACTERIZATION OF FIRMNESS AND DIELECTRIC PERMITTIVITY

The variation of the flesh firmness and the complex permittivity of the avocado as well as the ripening process were preliminarily evaluated by an experimental campaign involving both mechanical and electromagnetic measurements. The resulting data were then used for the design of the sensing system and to populate the data set for the training and testing of the classification algorithm, as described in the following.

FIRMNESS

Avocado fruits (the Hass cultivated variety from Mexico) were selected for their absence of defects, uniform appearance (size and color), and firmness. Mechanical tests were carried out on a set of 300. The fruits were stored in the dark at temperatures $T_e = \{7, 15, 20\}$ °C for different periods (seven to 10 days). Measurements of the weight loss, skin and flesh color, flesh firmness, and dry matter were done on a daily basis for five or six fruits. In particular, the flesh firmness was considered the reference parameter to evaluate and classify the ripening degree. It was measured into the pulp of the fruit by means of a Shore durometer (T.R. Turoni, Italy, 53215). Eight measurements were collected for each fruit, from both the basal and the equatorial areas, and properly averaged. The Shore values (SH) ranged between SH = 90 (unripe) and SH = 10 (ripe). Figure 1(a) displays the measured SH (the average and the standard deviation for fruits tested on the same day) for the three environmental conditions and referred to the basal region.

The intrinsic SH variability among fruits is not negligible, especially in cases of storage at cold temperatures [the standard deviation averaged on the daily tested fruit set was $\hat{\sigma}(7\ °C) = 16.4$; $\hat{\sigma}(15\ °C) = 7$; $\hat{\sigma}(20\ °C) = 13.6$)]. The ripening process evolves through time, with a progressive decrease of the flesh firmness that proceeds irregularly due to fruits' variability. This behavior further confirms the need for classification based on the combined exploitation of both the temporal and the RF indicators, as better explained in the following sections. The storage temperature has a boosting effect on the ripening time, raising ($T_e = 20$ °C) or lowering ($T_e = 7$ °C) the slope of the curves, especially early in the process. According to the SH levels, three classes (C) of ripening [Figure 1(b)] are defined (Table 1).

COMPLEX PERMITTIVITY

The dielectric properties $\{\epsilon_r, \sigma[S/m]\}$ of avocados along with ripening were measured by an open-ended coaxial probe

TABLE 1. RIPENING CLASSES VERSUS TEMPERATURES AND ELAPSED DAYS.

		Elapsed Days		
	SH	$T_e = 7$ °C	$T_e = 15$ °C	$T_e = 20$ °C
$C1$ (unripe)	70–90	1–6	1–3	1
$C2$ (ripe)	30–70	7–10	4–6	2–5
$C3$ (overripe)	10–30	>10	7–9	6–9

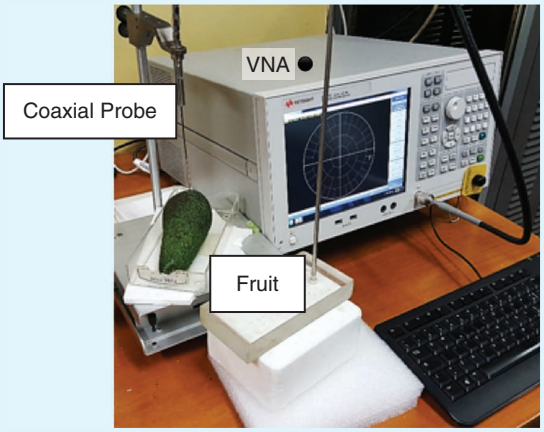

FIGURE 2. The setup for the avocado RF characterization. A VNA (Keysight ENA E5071C, 9 KHz–4.5 GHz) is connected to an open-ended coaxial probe (Keysight slim-form dielectric probe kit 85070E, with a 2.2-mm diameter and an approximately 3-mm penetration depth).

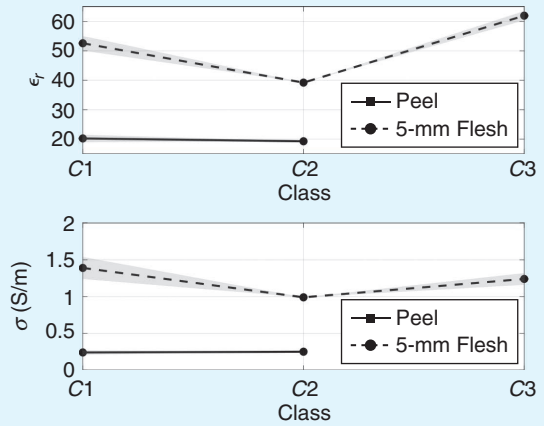

FIGURE 3. The measured dielectric properties of avocado versus ripening for two fruit locations. The averaged values at 870 MHz correspond to the three ripening states in Table 1. The shadowed area represents the standard deviation.

connected to a vector network analyzer (VNA) (Figure 2). Two different locations were considered, with the tip of the probe touching the external peel (average 2-mm thickness) of the basal region of the fruit and protruding into the pulp at a 5-mm depth. Nine fruits at three different maturation stages were considered (three for each class in Table 1). For each fruit, three measurements were performed in the 600–1,200-MHz frequency range.

The averaged results at 870 MHz are reported in Figure 3, together with the standard deviation, which is in gray. The measurements are quite stable. A dielectric contrast exists among the three states, with a nonmonotonic profile, consistent with the well-known physical/chemical variations described in the literature, which are nonmonotonic as well [27], [29], [30] (especially regarding the oil and sugar concentration). The percentage variation with respect to initial state *C*1 is moderate ($18\% < \Delta\epsilon_r < 25\%$ and $10\% < \Delta\sigma < 28\%$) and mainly limited to the pulp; the maturation process seems not to exert any appreciable electromagnetic effects on the peel, confirming the predominance of the chemical–physical variations of the fruit in the flesh [22]. When the fruit is overripe, the peel results are not measurable at all due to the extreme softening of the underlying structures, which prevents the firm adhesion of the coaxial probe to the fruit surface.

ELECTROMAGNETIC MODELING

The RFID-based avocado monitoring system in Figure 4(a) includes COTS elements. The reader antenna for the near-field coupling with the fruit is a segmented square loop (Advantenna-L11, Keonn [31]). It was selected for its compact size and very thin form factor, which is suitable for the integration within the RFID totem (described in the next section), and, above all, for the ability to focus and excite a strong, uniform electromagnetic field distribution within its detection zone (wherein the fruits are positioned). In fact, a segmented square loop layout facilitates keeping the current flowing along the loop at an almost equal magnitude and in-phase, resulting in a uniform field even though the loop is electrically large (comparable to the operating wavelength). Moreover, the selected reader antenna is quite broadband (with a frequency range of 813–1,000 MHz), thus

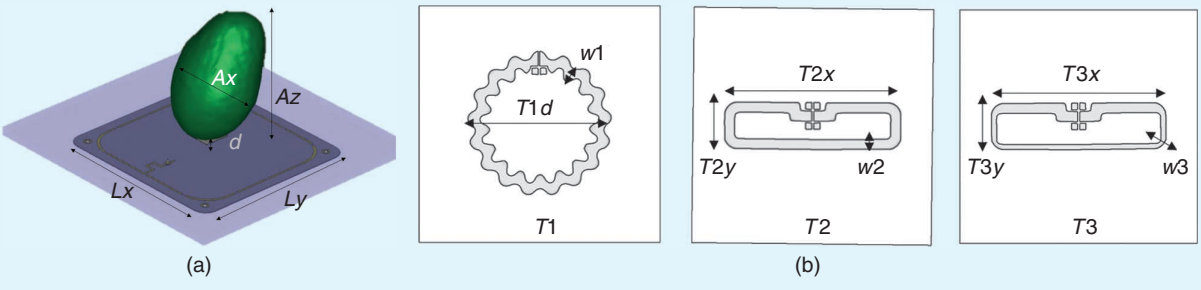

FIGURE 4. A model of the RFID monitoring system. (a) An avocado and the segmented square loop that serves as the reader antenna. The sizes are (in centimeters): $Az = 9$, $Ax = 6$, $Lx = Ly = 13.7$, and $d = 1$. (b) The commercial off-the-shelf (COTS) tag layouts to be attached to the avocado. The sizes are (in millimeters): $T1d = 12$, $T2x = T3x = 15$, $T2y = T3y = 4$, $w1 = w2 = 1$, and $w3 = 0.5$.

enabling the system to collect RF indicators in the dual band: European Telecommunication Standards Institute and Federal Communications Commission.

The considered tags are small-size loops resembling conventional fruit stickers in terms of their shape and size. Three different COTS layouts, denoted as $T1$, $T2$, and $T3$, were preliminary considered [Mecstar Loopetto; Figure 4(b)]. They all integrate the Monza R6P IC, with $Z_{chip} = 1.3 + j55.6\,\Omega$ and a sensitivity of $p_C = -21$ dBm. This IC is provided with five states of self-tuning. The whole RFID link was modeled by the finite difference time domain method by using the Dassault Microwave Studio 2019 solver, with the twofold purpose of 1) selecting the most convenient tag layout and 2) evaluating the field strength surrounding the reader, where operators and users are present so that exposure compliance can be assessed.

The avocado was represented as a two-layer (peel and flush) stratification, whose dielectric properties were derived from Figure 3 to reproduce the three ripening states. The internal seed was neglected. Since the electromagnetic interactions between the reader and the tag occur in the near field, the RFID link was described by a two-port network [32] and by its self-$Z_{ii}[\Re]$ and mutual $Z_{ij}[\Re]$ impedances. Ports 1 and 2 refer to the terminals of the reader's antenna and to the fruit tag, respectively. This representation accounts for the possible impedance mismatch at both the reader–antenna port (due to the presence of the fruit) and the tag–antenna port (due to the mutual coupling between the two antennas). The ripening process will have an effect on the tag's self- and mutual impedances.

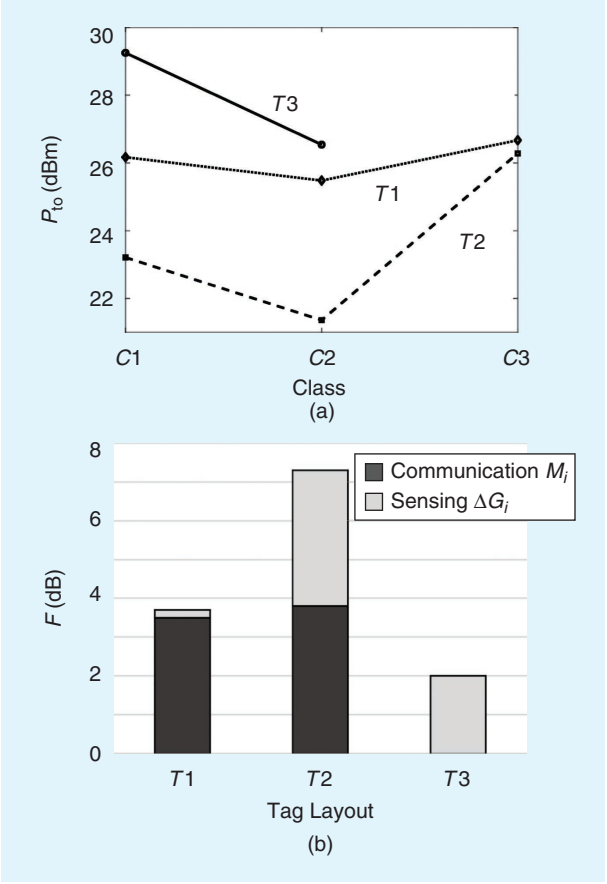

FIGURE 5. (a) The simulated turn-on power of the tagged avocado with a permittivity corresponding to the three maturation classes. (b) The fitness function F (dB) for the three tags accounting for communication and sensing.

The link is hence parameterized by the transducer power gain $G_T[\Re]$ [33], defined as

$$G_T[\Re] = \frac{P_{R\to T}[\Re]}{P_{av,R}} = \frac{4R_{chip}R_G|Z_{21}[\Re]|^2}{|(Z_{11}[\Re]+Z_G)(Z_{22}[\Re]+Z_{chip}) - Z_{12}[\Re]Z_{21}[\Re]|^2}, \quad (1)$$

where $R_G = 50\,\Omega$ is the internal resistance of the reader. Accordingly, the turn-on power can be expressed as $P_{to}[\Re] = p_c/G_T[\Re]$.

A reliable communication link can be established provided that the power emitted by the reader ($P_{av,R}$) is sufficient to deliver to the tag the energy requested to activate the microchip transponder. Indeed, sensing capabilities are generally achieved at the expense of the communication performance since the changes of the physical/chemical features of the fruit are sensed by the passive tag through a deviation from its unripe gain and/or impedance matching. Hence, the true effectiveness of the system descends from the tradeoff between sensing and communication.

Sensing requirements were imposed to maximize the dynamic range, i.e., the overall change of the measured parameters between the extreme $C1$ and $C3$ classes. Instead, ensuring a robust communication link regardless of the state of the process enforces a condition on the minimum turn-on power: $P_{to}(\Psi) \le P_{MAX}$ for $\Re \in \{C1, C2, C3\}$, where P_{MAX} is the upper-bound power in the reader's antenna; typically, $P_{MAX} = 30$ dBm. Figure 5(a) shows the numerically evaluated turn-on powers for the three tags, which exhibit different slopes and dynamic ranges. In line with the measured dielectric properties, all three sensing profiles are nonmonotonic. As discussed in the following, additional information and rules will be included in the classification to get rid of the nonmonotonicity of the electromagnetic indicators.

Tag selection is based on the maximization of the following fitness function:

$$F_{Ti} = M_{Ti}^{min} + \overline{\Delta P_{to,Ti}}, \quad (2)$$

where $M_{Ti}^{min} = P_{MAX} - P_{to,Ti}^{max}$ is the communication margin, where P_{to}^{max} is the maximum turn-on power across the three ripening states, and $\overline{\Delta P_{to,Ti}}$ is the average turn-on power variation between states $C1$ and $C3$ (sensing margin). Tag $T2$ resulted in the best configuration, with a minimum power margin of $M_{T2} = 3.8$ dB and a sensing range of $\overline{\Delta P_{to,T2}} = 3.5$ dB. Finally, the radiated electric field was evaluated in the surroundings of the fruit E_{rms} (root mean square values) corresponding to power $P_{in} = 0.25$ W in the reader's antenna (Figure 6). The field penetrates the fruit in its basal region. The system is compliant with

the European safety regulation, which is $E_{\text{rms}} \leq 41.3$ V/m [34] almost everywhere.

THE RFID TOTEM

The measurement setup was integrated in a scale-like RFID totem, including a ThingMagic M6e reader connected to the L11 Keonn near-field antenna, an embedded PC (Lattepanda) running custom software, and a touchscreen display. The overall cost of the assembled prototype is less than US$1,000. The software controls the measurement procedure, performs local processing of the retrieved data, applies machine learning techniques, (described in the following), and returns a visual indicator corresponding to the predicted ripening status of the fruit on the display. Additional information stored in the IC memory about the fruit origin and handling are displayed as well. The totem is, finally, provided with a plastic housing cradle to stably host the packaged fruit in a firm vertical or horizontal position (Figure 7), thus avoiding artifacts in the data retrieval due to the imperfect placement of the fruit [35].

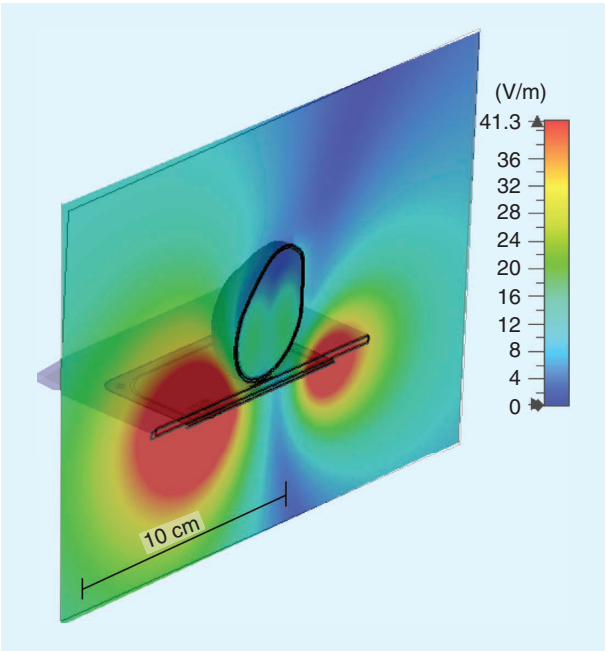

FIGURE 6. An example of the simulated field distribution around the avocado for the input power at the reader port equal to $P_{\text{in}} = 0.25$ W.

Avocados will be contained inside conformal Polyethylene terephthalate (PET) shells. The *T*2 tag is attached to the internal (basal or equatorial) side of the shells by means of a soft, 3-mm-thick neoprene foam substrate that guarantees the perfect adhesion of the tag to the peel of the fruit, regardless the variability of the fruit morphology (Figure 8). The reader antenna and tag will be therefore always aligned in parallel at a 1-cm distance. It is worth noting that the tag could be directly attached to the fruit peel, much like a standard fruit sticker. Such a configuration could offer better performance in terms of the quality of the collected RF signals, as the mutual position between the fruit and the tag is constant (not affected by the random movements of the fruit within the packaging), and the firm adhesion of the tag to the avocado makes the device more sensitive to dielectric changes (while the presence of a thin layer of air acts as a kind of "smoothing filter"). However, having the tag applied to the packaging enables supply chain applications beyond the ripeness evaluation, particularly "green"

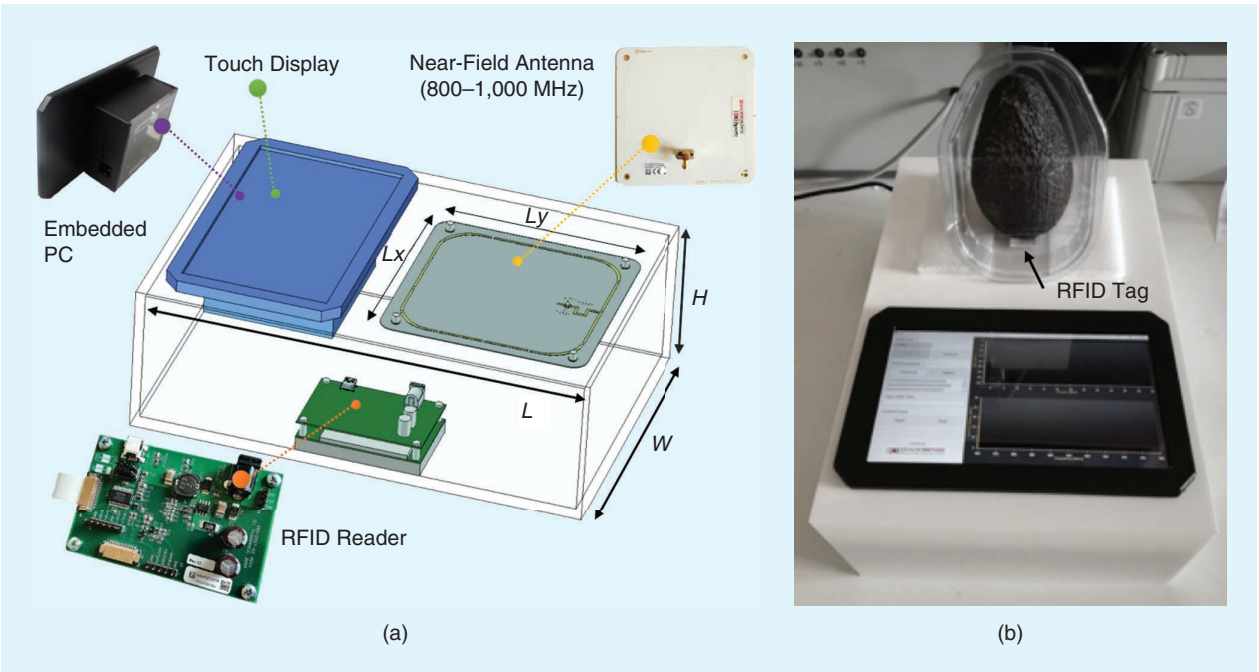

FIGURE 7. An exploded view of the RFID totem to monitor avocado ripening (The sizes, in centimeters, are $L = 30$, $W = 20$, and $H = 11$). (b) The fabricated prototype, with an avocado inside its smart packaging shell.

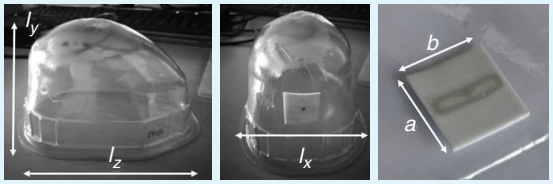

FIGURE 8. The intelligent packaging for avocados, including a PET shell and the *T*2 tag attached to the internal (basal or equatorial) side of the shell by means of soft, 3-mm-thick neoprene foam. The sizes are (in centimeters): $lx = 9.5$, $ly = 8$, $lz = 13.5$, and $a = b = 2$.

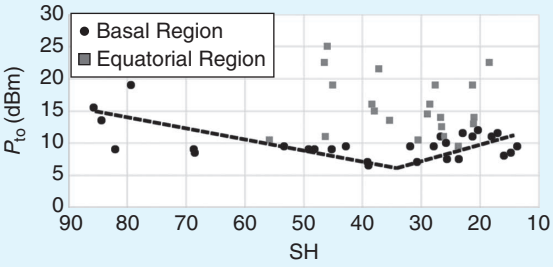

FIGURE 9. The P_{to} versus the SH for the *T*2 tags placed on both the basal and the equatorial regions of the fruit.

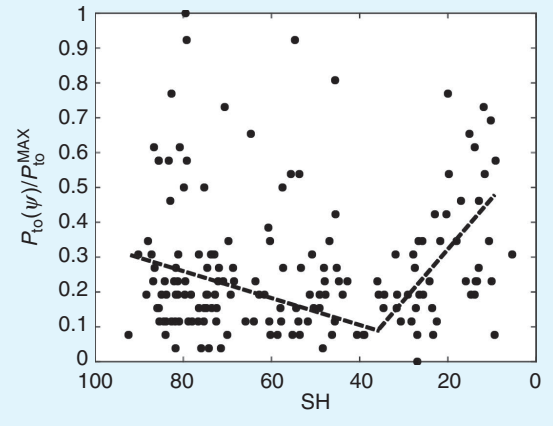

FIGURE 10. The normalized $P_{to}(\Psi)/P_{to}^{MAX}$ distribution for 163 avocados at different ripening stages.

solutions aimed at reducing plastic waste and incentivizing packaging recycling.

MEASUREMENT CAMPAIGNS

The RFID totem was first used in a preliminary measurement campaign involving a small set of fruits to evaluate two possible orientations of the avocado, with the tag placed on the basal and equatorial regions. In a second campaign, a larger number of fruits was considered to evaluate the accuracy and precision of the totem as a measurement instrument.

TEST 1: EVALUATION OF TAG POSITION

Measurements were performed on a set of 30 avocados. Tags were placed both in the basal and equatorial regions. Ripening was monitored along with time by measuring daily the evolution of the turn-on power P_{to} through the RFID totem. Three fruits were tested every day. For each one, the RF parameter was correlated to the flesh firmness SH measured by means of the durometer, as described previously, and then discarded (due to the destructiveness of the test). By initially focusing on the response of the basal-placed tags, the electromagnetic indicator undergoes variations along with the ripening process (as shown in Figure 9), thus confirming the rationale of the proposed approach. Despite the expected nonmonotonic trend (consistent with simulations), the sensing range is $\Delta P_{to} \approx 9$ dB, which is better than the numerical predictions. The communication is robust, with a margin of $M \geq 15$ dB across the entire ripening process. In the case of the equatorial-placed tags, the resulting data in terms of P_{to} (in Figure 9) are extremely dispersed. This effect is mainly due to the following reasons: 1) the fruits exhibit a great variability in their circumference and in the position of the pit within their flesh, 2) hence, it is difficult to have a standard package size with an inner housing that is able to wrap high around the circumference of the fruit, and 3) the ripening process is not homogenous along the equatorial section of the fruit. Consequently, this configuration will hereafter be discarded.

TEST 2: EVALUATION OF REPEATABILITY AND REPRODUCIBILITY

The robustness of the RFID totem was then assessed by evaluating the repeatability and reproducibility of the measurements. A large-scale measurement campaign was performed for 163 fruits tested at different ripening states. The standard deviations σ_P (for the repeatability) and σ_B (for the reproducibility) of the P_{to} indicator were evaluated. The repeatability was assessed by performing several measurements at the same time and under the same conditions, i.e., by keeping the whole arrangement of the system fixed (the position and orientation of the packaged fruit with respect to the totem). The reproducibility was assessed by performing measurements after placing the packaged fruit on, and removing it from, the totem. Such uncertainties are particularly relevant in case measurements are performed by unskilled operators (e.g., the final customer) that are not aware of the physical rationale of the system. For each fruit, the measurements have been repeated three times. In the worst case, $\sigma_P = 0.3$ dB and $\sigma_B = 0.5$ dB, which are comparable to typical RFID sensing systems [35], so the measurement design can be considered robust, and the uncertainties of the measurement itself look negligible.

Figure 10 presents the normalized turn-on power $p_{to} = P_{to}/P_{to}^{MAX}$ versus the SH. Despite the robustness of the setup, the measured data are rather spread, as fruits with a similar SH value return rather variable values of the turn-on power. Such a distribution confirms the high fruit variability and the possible jeopardizing effect on the ripening classification. Nevertheless, the same nonmonotonic trend as in Figure 9 is still visible.

CLASSIFICATION PROCEDURE

The prediction of the ripening classes $\{C1, C2, C3\}$ relies on machine learning techniques applied to the electromagnetic data collected by the RFID totem. A supervised classification algorithm was used, involving a two-step procedure, namely the training and testing phases. Among several possible classifiers [36], the decision tree is applied here for the easiness of its real-time implementation and its integration within the software controlling the RFID reader inside the totem. In a decision tree, data are continuously split according to a conditional relationship. Starting from the root, i.e., the input layer, a decision tree (Figure 11) consists of the following:

1) nodes labeled with the names of attributes
2) edges/branches labeled with the possible values of the attributes; they are represented as the arcs that connect to the next node or leaf
3) leaf nodes, which are terminal nodes that predict the outcome (they represent class labels); the sequential, hierarchical paths from root to leaf generate the classification rules.

Four topologies of heterogeneous data, collected by the totem, are used for building the classification model: 1) RF sensing parameters measured at the time t, $\{P_{R\to T}, P_{\text{to}}, \text{RSSI}\}$; 2) the packaging time t_0; 3) the fruit ripening stage $C_0 \in \{C1, C2, C3\}$ at the packaging time t_0; and, finally, 4) the storage temperature T_e (here, assumed to be constant between time t_0 and t). The first set of data (RF predictors) feeds the core of the detection algorithm, while the final three improve the accuracy of the classification by accounting for the natural evolution of the ripening along with time and the storage conditions (see Figure 11), which are known to have a strong impact on the ripening process (Figure 1). In particular, conditions 2–4 enforce the monotonic evolution of the ripening process $\{C1(t_1) \to C2(t_2) \to C3(t_3)$ with $t1 < t2 < t3\}$ through the following rules:

1) The fruit stage at the measurement time $t = t_m$ must follow the natural ripening process; e.g., if $C(t_{m-1}) = C2$, then $C(t_m) \in \{C2, C3\}$.

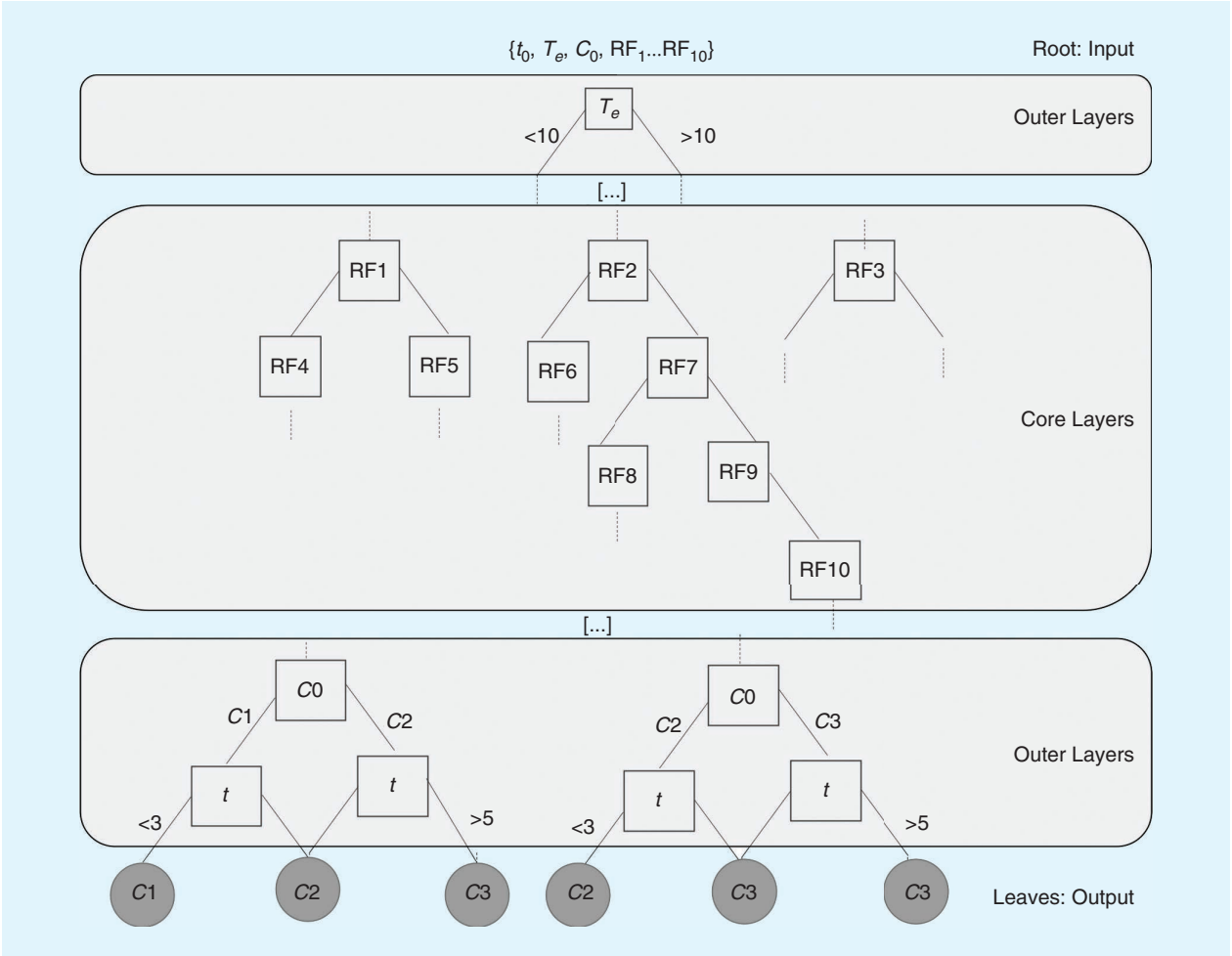

FIGURE 11. A schematic representation of the decision tree adopted for classifying avocado ripening. The tree consists of five groups of layers (here, for the sake of readability, the tree is not fully represented; some layers are hidden, and hence the groups are only logically connected). For each observation that enters the tree at the root layer, the set of features $\{t_0, T_e, C_0, \text{RF}_1 \ldots \text{RF}_{10}\}$ starts to be processed through nodes (□) and edges (\) to arrive at the output layer, where each leaf (○) represents a classified ripening stage. The outer layers mainly rely on the physical predictors $\{t_0, T_e, C_0\}$, while the core layers are mainly based on RF features.

TABLE 2. SELECTED RF FEATURES.

	RF Predictors	Description
RF1	$P_{\text{to}}^{\text{ST}-\text{ON}}\vert_{865}$	Turn-on power at 865 MHz with self-tuning on
RF2	$P_{\text{to}}^{\text{ST}-\text{OFF}}\vert_{865}$	Turn-on power at 865 MHz with self-tuning off
RF3	$P_{\text{to}}^{\text{ST}-\text{ON}}\vert_{915}$	Turn-on power at 915 MHz with self-tuning on
RF4	$P_{\text{to}}^{\text{ST}-\text{OFF}}\vert_{915}$	Turn-on power at 915 MHz with self-tuning off
RF5	$\text{RSSI}_{\text{to}}^{\text{ST}-\text{ON}}\vert_{865}$	RSSI for $P_{\text{in}} = P_{\text{to}}$ at 865 MHz with self-tuning on
RF6	$\text{RSSI}_{\text{to}}^{\text{ST}-\text{OFF}}\vert_{865}$	RSSI for $P_{\text{in}} = P_{\text{to}}$ at 865 MHz with self-tuning off
RF7	$\text{RSSI}_{\text{to}}^{\text{ST}-\text{ON}}\vert_{915}$	RSSI for $P_{\text{in}} = P_{\text{to}}$ at 915 MHz with self-tuning on
RF8	$\text{RSSI}_{\text{to}}^{\text{ST}-\text{OFF}}\vert_{915}$	RSSI for $P_{\text{in}} = P_{\text{to}}$ at 915 MHz with self-tuning off
RF9	$\Delta P_{\text{to}}\vert_{865}$	$\Delta P_{\text{to}}\vert_{865} = P_{\text{to}}^{\text{ST}-\text{ON}}\vert_{865} - P_{\text{to}}^{\text{ST}-\text{OFF}}\vert_{865}$
RF10	$\Delta P_{\text{to}}\vert_{915}$	$\Delta P_{\text{to}}\vert_{915} = P_{\text{to}}^{\text{ST}-\text{ON}}\vert_{915} - P_{\text{to}}^{\text{ST}-\text{OFF}}\vert_{915}$

2) According to the packaging date t_0, the elapsed time $\Delta t = t_m - t_0$ and the storage temperature T_e, the corresponding $t \leftrightarrow SH$ model derived in Figure 1 is applied.

It is worth noting that, thanks to the intrinsic functionalities of the RFID platform, the parameters $\{t_0, C_0, T_e, t_m, C_{t_m}\}$ can be automatically written inside the IC memory during the different phases of the fruit distribution and dynamically updated many times, from the orchard to retail, thus being available at any time along the chain for feeding the classification algorithm.

The classification task includes the collection of a data set to be used for both the training and the testing, choosing the minimum number of appropriate features to be extracted from the raw data, and evaluating the classifier accuracy. During training, the classification algorithm builds the decision tree. Starting from the root, the tree progressively branches by adding the different nodes and the relative edges and establishing the proper attribute-based conditions. After training, the accuracy of the prediction model is evaluated on the testing data set by comparing the known category labels with those obtained from the model.

At the end of this process, the classifier can be used to categorize new and unlabeled data. Results of the classification are summarized by the confusion matrix (CM): a 3×3 table that describes the relationships between the estimated and real patterns, i.e., the ability to correctly classify the ripening class $\{C1, C2, C3\}$. The CM is built from the testing data set, which has not been used for training, where the correct labels are known. In particular, the CM(p, q) element of the matrix indicates the normalized occurrences when an event of the pth class is classified as belonging to the qth class. The classification system is more accurate since the CM is diagonal. The accuracy A of a classifier is, then, the percentage of the observations that are correctly estimated. It can be easily derived from the CM as the ratio of the sum of the diagonal elements divided by the sum of all the elements.

TRAINING AND TEST

A data set has been built by measuring more than 300 avocados. Each fruit was assigned to a ripening class according to the measured SH and the scheme in Table 1. RF parameters $\{P_{R\rightarrow T}, P_{\text{to}}, \text{RSSI}\}$ were measured through the RFID totem and processed to extract 26 features (the sensor code proved to be barely effective, and hence it was discarded). Among them, a subset of 10 have been selected to feed the algorithm (the details are in Table 2, and an example of the measured data is given in Figure 12). It is worth noting that the RF features were measured at two frequencies (865 and 915 MHz) to enrich the available data set. Indeed, despite the modest variability of the dielectric properties of fruit pulp in the UHF RFID band, the RFID tag works differently (see Figure 12) due to the frequency-dependent performance of the loop antenna and of the connected IC as well as the different near-field interaction of the reader antenna with the fruit matter. Accordingly, other useful information is expected.

The fruit fingerprint, including predictors and results, is

$$\{t_0, T_e, C_0, \text{RF}_1 \ldots \text{RF}_{10}; C_m\}, \tag{3}$$

where C_m is the classification response, namely the ripening class at time t_m. Overall, a data set of roughly 4,200 entries was generated. The classical k-fold technique was used for both the training and the testing. The data set was randomly split into k = 10 subsets, denoted as folds: $(k-1)$ folds are used for the training, and the remaining set is employed for the validation. The procedure is then repeated k times by sequential rotation until each partition has been used for the test.

The resulting CM is in Figure 13(a). The overall accuracy was $A = 83\%$, with the extremal classes $C1$ and $C3$ particularly well discriminated (80–90%). Thanks to the enforced temporal evolution of the ripening process, the misclassification events between two adjacent classes are less than 20%, thus limiting the impact of a wrong estimation for the final user. For the sake of completeness, it is worth reporting that by considering only the RF features, the maximum achievable accuracy never exceeds 65–70%, while relying exclusively on the physical indicators (time and temperature) led to a very variable performance, with the accuracy ranging from 30 to 90%.

AN EXAMPLE APPLICATION

An example of automatic classification performed on a new set of 188 avocados, which were not included in the training task, is finally reported in Figure 13(b). In this experiment, the RFID totem was used by a generic operator who was not aware of the electromagnetic issues so that the test could be considered

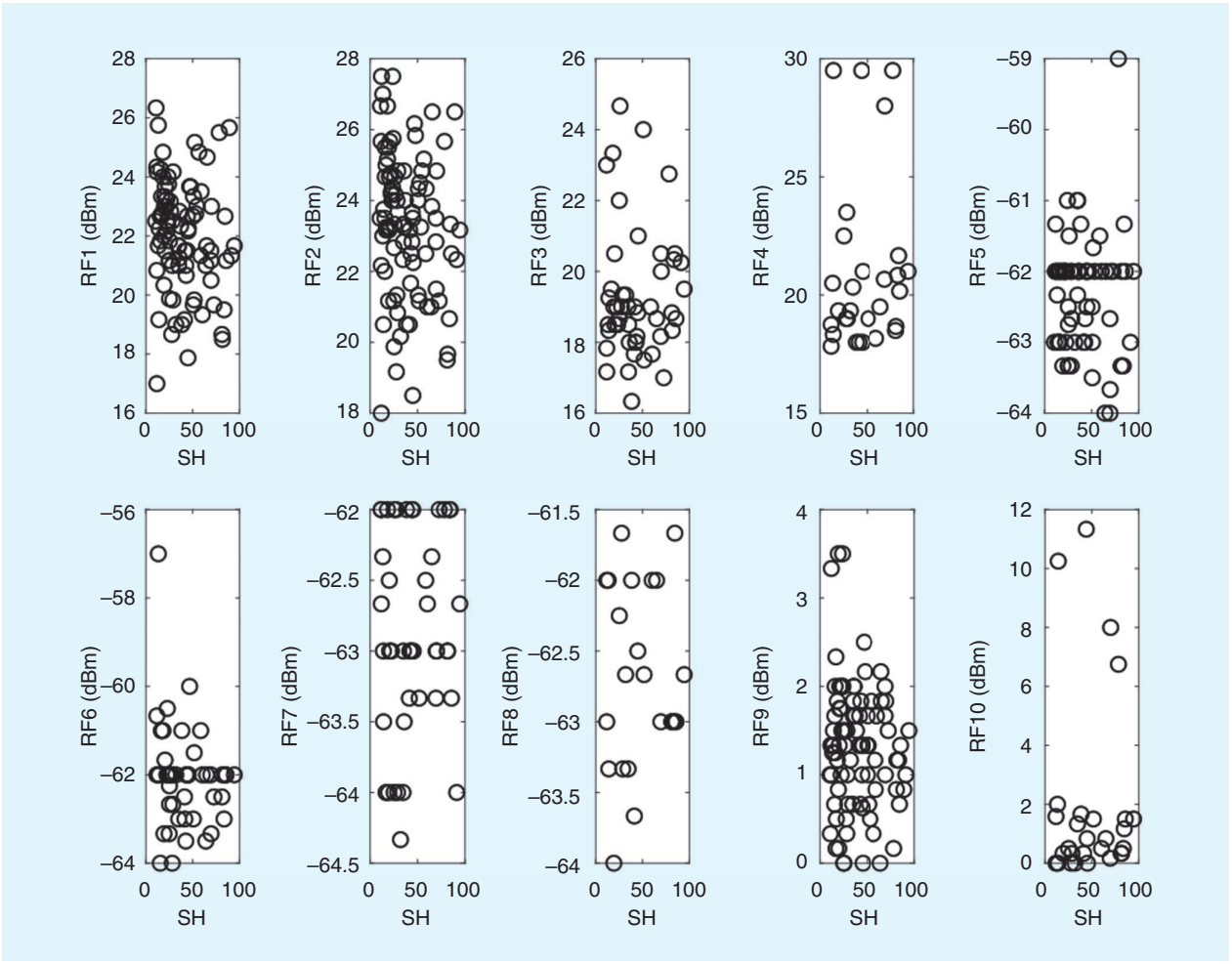

FIGURE 12. An example of the 10 measured RF features.

blind and realistic. The resulting CM is still mostly diagonal. As expected, by the added rules, misclassification events occur only among adjacent classes, with an overall accuracy of $A = 90\%$.

CONCLUSIONS

This article proposed a batteryless RFID sensing system for avocado ripening assessment that aimed to define the best time to eat the fruit, optimize the produce's exposition on store shelves, and reduce retail waste. The UHF RFID tag integrated within the packaging acts as an electromagnetic transducer that converts the chemical–physical modification of fruits during ripening into a modulation of the electromagnetic parameters that can be revealed at the reader side. Measured data then undergo an automatic classification procedure based on decision trees that are able to predict a three-level state of the fruit: unripe, ripe, and overripe.

Based on experimental tests on more than 300 fruits, a classification accuracy greater than 85% can be achieved provided that, besides the electromagnetic indicators, information about the storage temperature and the initial condition at the packaging time are accounted for in the model to get rid of the natural nonmonotonic evolution of the constitutive electromagnetic parameters during ripening and, above all, of the variability fruits. Richer SH–time–temperature models accounting for several storage ambient conditions are expected to further improve the detection capabilities of the system. Finally, the described system is expected

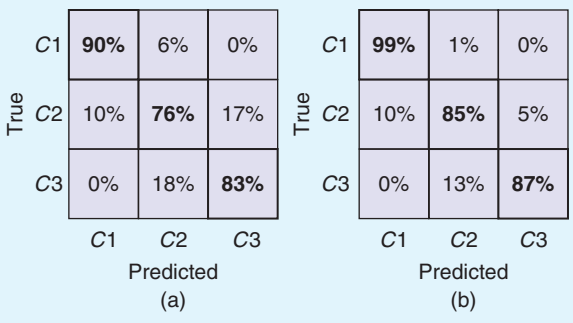

FIGURE 13. The confusion matrices of the avocado ripening classification that result from the binary tree analysis. (a) N.300 fruits used for both the training and the test, with controlled measurements made by expert operators. (b) N.188 fruits used only for the classification, with measurements made by generic operators.

to be straightforwardly applicable to any perishable food whose chemical/physical features change significantly with the time, provided that the classification tree is properly trained across the corresponding data sets. Early experiments involving other tropical fruits, such as mangos and papayas, are currently ongoing.

ACKNOWLEDGMENTS

The authors thank Dr. Vanni Lopresto for supporting the measurement of the avocado electromagnetic parameters and Prof. Eugenio Martinelli and Michele D'Orazio for their useful discussions and support with the classification methods.

AUTHOR INFORMATION

Cecilia Occhiuzzi (cecilia.occhiuzzi@uniroma2.it) is an assistant professor at the University of Rome "Tor Vergata" and cofounder and chief executive officer of RADIO6ENSE. Her research interests include wireless health monitoring by means of wearable and implantable radio-frequency/millimeter-wave identification techniques and pervasive-sensing paradigms for Industry 4.0. She is a Member of IEEE.

Nicola D'Uva (duva@radio6ense.com) is a radio-frequency engineer at RADIO6ENSE. His research interests include the industrial Internet of Things and electronics for harsh environments.

Simone Nappi (Simone.nappi@uniroma2.it) is a Ph.D. student in computer science, control, and geoinformation. His research interests include sensing systems for automotive and production sectors.

Amendola Sara (amendola@radio6ense.com) is a project manager at RADIO6ENSE. Her research interests include epidermal electronics and sensing systems for Industry 4.0.

Chiara Gialluca (c.gialluca@ilip.it) is a member of the research and development group at ILIP. Her research interests include smart packaging technologies and quality control.

Valentina Chiabrando (valentina.chiabrando@unito.it) is with the Department of Agricultural, Forestry and Food Sciences, University of Torino. Her research interests include the postharvest quality of whole and fresh-cut fruits and postharvest treatments aimed to control fruit quality losses.

Luigi Garavaglia (l.garavaglia@ilpagroup.com) is the research and development manager at ILIP. His research interests include smart systems for food packaging and quality control.

Giovanna Giacalone (giovanna.giacalone@unito.it) is with the Department of Agricultural, Forestry and Food Sciences, University of Torino. Her main research interests include whole and fresh-cut fruit quality and postharvest management.

Gaetano Marrocco (gaetano.marrocco@uniroma2.it) is a full professor at the University of Rome "Tor Vergata," where he also serves as director of the Medical Engineering School. He is also the cofounder and president of RADIO6ENSE. His research interests include epidermal electronics and wireless sensing systems for biomedical engineering, aeronautics, and radio-frequency identification. He is a Member of IEEE.

REFERENCES

[1] S. Kalpana, S. Priyadarshini, M. M. Leena, J. Moses, and C. Anandharamakrishnan, "Intelligent packaging: Trends and applications in food systems," *Trends Food Sci. Technol.*, vol. 93, pp. 145–157, Nov. 2019. doi: 10.1016/j.tifs.2019.09.008.

[2] M. Ghaani, C. A. Cozzolino, G. Castelli, and S. Farris, "An overview of the intelligent packaging technologies in the food sector," *Trends Food Sci. Technol.*, vol. 51, pp. 1–11, May 2016. doi: 10.1016/j.tifs.2016.02.008.

[3] P. Butler, "10: Smart and interactive packaging developments for enhanced communication at the packaging/user interface," in *Trends in Packaging of Food, Beverages and Other Fast-Moving Consumer Goods (FMCG)* (Series in Food Science, Technology and Nutrition), N. Farmer, Ed. Sawston, U.K.: Woodhead Publishing, 2013, pp. 261–287.

[4] J. M. Soon and L. Manning, "Developing anti-counterfeiting measures: The role of smart packaging," *Food Res. Int.*, vol. 123, pp. 135–143, Sept. 2019. doi: 10.1016/j.foodres.2019.04.049.

[5] M. G. Corradini, "Shelf life of food products: From open labeling to real-time measurements," *Annu. Rev. Food Sci. Technol.*, vol. 9, pp. 251–269, Mar. 2018. doi: 10.1146/annurev-food-030117-012433.

[6] M. F. F. Poças, T. F. Delgado, and F. A. R. Oliveira, "Smart packaging technologies for fruits and vegetables," in *Smart Packaging Technologies for Fast Moving Consumer Goods*, J. Kerry and P. Butler, Eds. Hoboken, NJ: Wiley, 2008, ch. 9, pp. 151–166.

[7] Z. Fang, Y. Zhao, R. D. Warner, and S. K. Johnson, "Active and intelligent packaging in meat industry," *Trends Food Sci. Technol.*, vol. 61, pp. 60–71, Mar. 2017. doi: 10.1016/j.tifs.2017.01.002.

[8] V. Chonhenchob, W. Chinsirikul, and S. Singh, "Current and innovative packaging technologies for tropical and subtropical fruits," in *Tropical and Subtropical Fruits: Postharvest Physiology, Processing and Packaging*, M. Siddiq, Ed. Hoboken, NJ: Wiley, 2012, pp. 115–134.

[9] P. Taoukis and T. Labuza, "6: Time-temperature indicators (TTIs)," in *Novel Food Packaging Techniques* (Series in Food Science, Technology and Nutrition), R. Ahvenainen, Ed. Sawston, U.K.: Woodhead Publishing, 2003, pp. 103–126.

[10] F. Bibi, C. Guillaume, N. Gontard, and B. Sorli, "A review: RFID technology having sensing aptitudes for food industry and their contribution to tracking and monitoring of food products," *Trends Food Sci. Technol.*, vol. 62, pp. 91–103, Apr. 2017. doi: 10.1016/j.tifs.2017.01.013.

[11] K. Finkenzeller, *RFID Handbook: Fundamentals and Applications in Contactless Smart Cards and Identification*, 2nd ed. Hoboken, NJ: Wiley, 2003.

[12] S. Mondal, K. P. Wijewardena, S. Karuppuswami, N. Kriti, D. Kumar, and P. Chahal, "Blockchain inspired RFID-based information architecture for food supply chain," *IEEE Internet Things J.*, vol. 6, no. 3, pp. 5803–5813, June 2019. doi: 10.1109/JIOT.2019.2907658.

[13] C. Occhiuzzi, S. Caizzone, and G. Marrocco, "Passive UHF RFID antennas for sensing applications: Principles, methods, and classifcations," *IEEE Antennas Propag. Mag.*, vol. 55, no. 6, pp. 14–34, Dec. 2013. doi: 10.1109/MAP.2013.6781700.

[14] S. Caizzone, C. Occhiuzzi, and G. Marrocco, "Multi-chip RFID antenna integrating shape-memory alloys for detection of thermal thresholds," *IEEE Trans. Antennas Propag.*, vol. 59, no. 7, pp. 2488–2494, 2011. doi: 10.1109/TAP.2011.2152341.

[15] C. Occhiuzzi, A. Rida, G. Marrocco, and M. M. Tentzeris, "CNT-based RFID passive gas sensor," in *Proc. 2011 IEEE MTT-S Int. Microwave Symp.*, June 2011, pp. 1–4. doi: 10.1109/MWSYM.2011.5972715.

[16] S. Manzari, A. Catini, G. Pomarico, C. D. Natale, and G. Marrocco, "Development of an UHF RFID chemical sensor array for battery-less ambient sensing," *IEEE Sensors J.*, vol. 14, no. 10, pp. 3616–3623, Oct. 2014. doi: 10.1109/JSEN.2014.2329268.

[17] S. Manzari, C. Occhiuzzi, S. Nawale, A. Catini, C. Di Natale, and G. Marrocco, "Humidity sensing by polymer-loaded UHF RFID antennas," *IEEE Sensors J.*, vol. 12, no. 9, pp. 2851–2858, 2012. doi: 10.1109/JSEN.2012.2202897.

[18] C. Amador, J.-P. Emond, and M. C. do Nascimento Nunes, "Application of RFID technologies in the temperature mapping of the pineapple supply chain," *Sens. Instrum. Food Qual. Saf.*, vol. 3, pp. 26–33, Mar. 2009. doi: 10.1007/s11694-009-9072-6.

[19] A. Abdelnour, N. Fonseca, A. Rennane, D. Kaddour, and S. Tedjini, "Design of RFID sensor tag for cheese quality monitoring," in *Proc. 2019 IEEE MTT-S Int. Microwave Symp. (IMS)*, June 2019, pp. 290–292. doi: 10.1109/MWSYM.2019.8700769.

[20] B. Saggin, Y. Belaizi, A. Vena, B. Sorli, V. Guillard, and I. Dedieu, "A flexible biopolymer based UHF RFID-sensor for food quality monitoring," in *Proc. 2019 IEEE Int. Conf. RFID Technology Applications (RFID-TA)*, Sept. 2019, pp. 484–487. doi: 10.1109/RFID-TA.2019.8892248.

[21] S. D. Nguyen, T. T. Pham, E. Fribourg Blanc, N. Nguyen Le, C. M. Dang, and S. Tedjini, "Approach for quality detection of food by RFID-based wireless sensor tag," *Electron. Lett.*, vol. 49, no. 25, pp. 1588–1589, Dec. 2013. doi: 10.1049/el.2013.3328.

[22] B. Schaffer, B. N. Wolstenholme, and A. W. Whiley, *The Avocado: Botany, Production and Uses*, 2nd ed. Wallingford, U.K.: CABI, 2013.

[23] P. Magdalita and L. Valencia, "Fruit variability and correlation analysis of some phenotypic characters in avocado (Persea americana Mill.), rambutan

(Nephelium lappaceum L.) and sweetsop (Annona squamosa L.)," *Philipp. Agric. Sci.*, vol. 87, no. 4, pp. 463–467, 2004.
[24] A. A. Kader, "Fruit maturity, ripening, and quality relationships," *Acta Hortic.*, vol. 485, pp. 203–208, Mar. 1999. doi: 10.17660/ActaHortic.1999.485.27.
[25] P. J. Hofman, B. A. Stubbings, M. F. Adkins, R. J. Corcoran, A. White, and A. B. Woolf, "Low temperature conditioning before cold disinfestation improves 'Hass' avocado fruit quality," *Postharvest Biol. Technol.*, vol. 28, no. 1, pp. 123–133, 2003. doi: 10.1016/S0925-5214(02)00175-8.
[26] J. Villa-Rodriguez, F. J. Molina-Corral, J. F. Ayala-Zavala, G. Olivas, and G. Aguilar, "Effect of maturity stage on the content of fatty acids and antioxidant activity of 'Hass' avocado," *Food Res. Int.*, vol. 44, no. 5, pp. 1231–1237, 2011. doi: 10.1016/j.foodres.2010.11.012.
[27] D. E. Khaled, N. Novas, J.-A. Gazquez, R. M. Garcia, and F. Manzano-Agugliaro, "A fruit and vegetable quality assessment via dielectric sensing," *Sensors*, vol. 15, no. 7, pp. 15,363–15,397, 2015. doi: 10.3390/s150715363.
[28] M. C. Caccami and G. Marrocco, "Electromagnetic modeling of self-tuning RFID sensor antennas in linear and nonlinear regimes," *IEEE Trans. Antennas Propag.*, vol. 66, no. 6, pp. 2779–2787, June 2018. doi: 10.1109/TAP.2018.2820322.
[29] D. Ahmed, A. Yousef, and H. Hassan, "Relationship between electrical conductivity, softening and color of Fuerte avocado fruits during ripening," *Agric. Biol. J. N. Am.*, vol. 1, no. 5, pp. 878–885, 2010. doi: 10.5251/abjna.2010.1.5.878.885.
[30] M. Montoya, J. D. L. Plaza, and V. Lopez-Rodriguez, "Electrical conductivity of avocado fruits during cold storage and ripening," *LWT-Food Sci. Technol.*, vol. 27, no. 1, pp. 34–38, 1994. doi: 10.1006/fstl.1994.1008.
[31] "L11 Near Field antenna," Keonn Technologies, Barcelona, Spain, 2020. [Online]. Available: https://www.keonn.com/images/stories/pdf/Keonn-Advantenna-L11-Data_sheet.pdf
[32] S. Amendola, V. Di Cecco, and G. Marrocco, "Numerical and experimental characterization of wrist-fingers communication link for RFID-based finger augmented devices," *IEEE Trans. Antennas Propag.*, vol. 67, no. 1, pp. 531–540, Jan. 2019. doi: 10.1109/TAP.2018.2876703.
[33] S. Orfanidis, *Electromagnetic Waves and Antennas*. New Brunswick, NJ: Rutgers Univ., Aug. 2010.
[34] European Commission, "1999/519/EC: Council Recommendation of 12 July 1999 on the limitation of exposure of the general public to electromagnetic fields (0 Hz to 300 GHz)," document 31999H0519, 1999.
[35] C. Occhiuzzi and G. Marrocco, "Precision and accuracy in UHF-RFID power measurements for passive sensing," *IEEE Sensors J.*, vol. 16, no. 9, pp. 3091–3098, 2016. doi: 10.1109/JSEN.2016.2526678.
[36] T. Hastie, R. Tibshirani, and J. Friedman, *The Elements of Statistical Learning*, 2nd ed. New York: Springer-Verlag, 2009.